

Pore Structure of Hard Carbon Made from Phenolic Resin Studied by ^{129}Xe NMR

Kazuma Gotoh,*[1] Takahiro Ueda,[2] Taro Eguchi,[2] Koji Kawabata,[3] Kenji Yamamoto,[1] Yuki Murakami,[1] Satoshi Hayakawa,[1] and Hiroyuki Ishida[1]

[1]Graduate School of Natural Science and Technology, Okayama University, Okayama 700-8530

[2]The Museum of Osaka University, Osaka University, Toyonaka, Osaka 560-0043

[3]Industrial Technology Center of Okayama Prefecture, 5301 Haga, Okayama 701-1296

Received February 3, 2009; E-mail: kgotoh@cc.okayama-u.ac.jp

The pore structure of hard carbon samples made from two kinds of phenolic resins by heating between 1073 and 1473 K was investigated by ^{129}Xe NMR. The difference of porous structure of hard carbon samples by heat treatment temperature, which was difficult to analyze precisely by general gas adsorption methods, could be evaluated by Xe NMR at an equilibrium state of xenon gas adsorption. Carbon samples produced by heating precursors under a 0.1 MPa xenon atmosphere showed stronger NMR signals than carbon heated at reduced pressure, despite their almost identical powder X-ray diffraction (XRD) patterns. Applying this method, the dependence of NMR spectra on heating temperature between 1073 and 1473 K was examined. A carbon sample consisting of smaller particles showed almost constant shift values at about 102 ppm, while the peak of another sample with larger particles shifted between 118 and 82 ppm depending on the heating temperature. Then, almost all entrances of each sample closed above 1273 K. Using NMR with the improved heat-treatment by xenon gas, we evaluated pores in hard carbon that were hard to access from the outer surface of the hard carbon.

Amorphous carbon has been applied to many industrial uses such as carbon black, carbon fiber, and activated carbon. The uses are rapidly developing and expanding with the advance of higher technology. One amorphous carbon material, non-graphitizable carbon (hard carbon), is expected to be an anode active material suitable for use in lithium ion secondary batteries for large devices such as hybrid electric vehicles because of the characteristics described below.[1–3] The primary advantages of a hard carbon anode are high charge and discharge rates and high durability with small volume change, resulting from the pore structure of the hard carbon. The pore structure of hard carbon depends on the kind of thermosetting resins used as the starting material and the temperature of preparation.[4,5] Generally, hard carbon shrinks with increasing heat-treatment temperature up to 1573 K, but shrunken carbon heated to over 2273 K still has pores, which are gas-impermeable. The closed pore diameter of carbon heat-treated at 1273–3273 K is estimated to be 2–5 nm using X-ray small-angle scattering.[6,7] Even in hard carbons, it is difficult to evaluate pore size using a common gas adsorption method, because a very long time is spent reaching the adsorption–desorption equilibrium (a few days to over a week).

On the other hand, the local structure of lithium electrochemically intercalated in hard carbon and its relationship to the pore structure have been investigated by Li NMR.[3,8–10] In our previous study of some pitch-based hard carbon samples for battery use,[3] the intensity of NMR signals of quasimetallic lithium clusters was nearly proportional to the amount of lithium in the pores of carbon estimated from charge–discharge curves. However, the size of quasimetallic lithium clusters and pores could not be evaluated. Tatsumi et al.[11] and Conard et al.[8] have observed the lithium clusters only in hard carbon samples heat-treated at about 1273–1573 K. This suggests that the pores where lithium clusters are formed are essentially different from those observed by X-ray small-angle scattering.

Recently, some different approaches have been reported, for example, small-angle neutron scattering,[12] and our ^{129}Xe NMR.[13] The former implied that a void between graphene sheets expands with lithium intercalation. By use of ^{129}Xe NMR, we could observe xenon permeable pores in the pitch-based hard carbon using ^{129}Xe NMR.[13] ^{129}Xe NMR has been recognized as a powerful method to evaluate porous structures.[14,15] It has been applied to various materials, for example, zeolites[16–24] and the other microporous and mesoporous materials,[25–31] hydrates,[32,33] glasses,[34] polymers,[35–40] and carbon materials such as fullerenes,[41,42] nanotubes,[43–45] and porous (activated) carbons.[46–50] Our high-pressure Xe NMR measurements[13] showed that the hard carbon samples in Xe gas had two peaks, which were attributed to the xenon in micropores (smaller than 1 nm) and larger pores (mesopores and macropores). The former peak was, however, very weak in spite of more than 30000 scans; therefore, pressure dependence of the peak was not observed. Treatment by evacuation at 773 K and annealing in 0.1 MPa Xe gas at 773 K also caused weak peaks of xenon confined in micropores of hard carbon, and transformation of surface structure was observed.

In the present study, we intended to construct a method for investigating the transition of pore structure of hard carbon

Published on the web October 8, 2009; doi:10.1246/bcsj.82.1232

heated at 1073–1473 K, which is the range of gradual shrinkage of carbon, using ^{129}Xe NMR. We choose two pre-heated spherical phenolic resins having different particle sizes and surface areas as heating precursors, and then heated at 1073–1473 K under reduced pressure or in xenon atmosphere for the purpose. We also compared the present samples with other carbons produced by different precursors by Xe NMR. The produced samples were measured by ^{129}Xe NMR, field emission scanning electron microscopy (FE-SEM), powder X-ray diffraction (XRD), and nitrogen adsorption. The effect of heating or annealing in xenon atmosphere was also investigated.

Experimental

Sample Preparation. Two kinds of spherical phenolic resins (Bellpearl R100 and Bellpearl R700 from Air Water Inc., hereafter named resin A and resin B, respectively) were used as raw materials. The radii of resin A and B are ca. 0.7 and 7 μm. Pre-heated carbon materials (named pre-heated resin A and pre-heated resin B) were prepared, respectively, by heating resin A and B at 873 K in nitrogen gas. Carbon samples for the NMR measurement were made from pre-heated resins A and B by heating at 1073, 1273, and 1473 K for 1.5 h in Xe atmosphere. The carbon samples made from pre-heated resins A and B in Xe atmosphere are respectively named carbon$_{Xe}$ A and carbon$_{Xe}$ B. Samples heated at 1273 and 1473 K under reduced pressure (≈0.1 Pa) for 1.5 h were also prepared from pre-heated resins A and B. The carbon samples made by heating pre-heated resins A and B under reduced pressure are respectively named carbon$_{rp}$ A and carbon$_{rp}$ B. All specimens were taken out from the furnace after cooling down and preserved in air.

To examine the annealing effect at 773 K in Xe gas, carbon$_{Xe}$ A heated at 1273 and 1473 K were evacuated at 773 K for 24 h and exposed to 0.1 MPa Xe gas at 773 K for 24 h. These samples were designated as "annealed carbon$_{Xe}$ A."

^{129}Xe NMR Measurement at Atmospheric Pressure and ESR. Each specimen was evacuated at 0.1 Pa at 373 K and then sealed in 9 mmϕ glass sample tubes at room temperature with Xe gas at 0.1 MPa for NMR measurements. All ^{129}Xe NMR spectra were recorded at room temperature using a spectrometer (55.6 MHz, MSL-200; Bruker Analytik GmbH) with a normal probe for liquid samples. The 0.1 MPa Xe gas signal was used as the 0-ppm standard for the ^{129}Xe NMR chemical shift. A single pulse sequence with a pulse delay of 5 s and a $\pi/2$ pulse of 4 μs were used for measurements. The pulse delay of 5 s was confirmed to be sufficient by monitoring signal intensities. Each spectrum was acquired in 1000–2000 scans. ESR spectra were measured for the heated carbon samples to investigate the magnetism, using a JES-FE3XG (JEOL Ltd.) spectrometer.

XRD, Nitrogen Gas Adsorption, FE-SEM, and Elemental Analysis. Powder X-ray diffraction (XRD) patterns were measured using a diffractometer (MultiFlex; Rigaku Corp.) with Cu Kα radiation. Although we tried to measure nitrogen gas adsorption–desorption isotherms for all samples by using Belsorp-18Plus (Bel Japan Inc.), only the data for carbon$_{Xe}$ A were successfully obtained. Other measurements failed due to excessive adsorption time as described in the following results and discussion. The BET surface areas of samples were estimated with the same instrument (Belsorp-18Plus). The shapes of carbon$_{Xe}$ A and B were observed using FE-SEM (JSM-7500F; JEOL) with 5.0 kV of access voltage. The composition of each sample heated over 873 K was measured by elemental analysis.

Table 1. BET Surface Area of Pre-Heated Resin A, Pre-Heated Resin B, Carbon$_{Xe}$ A (Heated in Xe Gas), and Carbon$_{Xe}$ B (Heated in Xe Gas)[a)]

	Pre-heated at 873 K	Heating temperature/K	
		1273	1473
Surface area of carbon$_{Xe}$ A/m^2 g^{-1}	475	250	7.8
Surface area of carbon$_{Xe}$ B/m^2 g^{-1}	6.7	144	1

a) These are reliable minimum values because equilibrium was not completely established for each point of isotherms due to long adsorption time.

Table 2. BET Surface Area of Pre-Heated Resin A, Pre-Heated Resin B, Carbon$_{rp}$ A (Heated under Reduced Pressure), and Carbon$_{rp}$ B (Heated under Reduced Pressure)[a)]

	Pre-heated at 873 K	Heating temperature/K	
		1273	1473
Surface area of carbon$_{rp}$ A/m^2 g^{-1}	475	306	15
Surface area of carbon$_{rp}$ B/m^2 g^{-1}	6.7	0.5	0.6

a) These are also reliable minimum values.

Results and Discussion

BET Surface Area and Isotherm. Table 1 shows the BET surface area of pre-heated resins and carbon$_{Xe}$ A and B. The surface area of pre-heated resin A (475 m^2 g^{-1}) was larger than that of pre-heated resin B (6.7 m^2 g^{-1}). This difference can be attributed to the particle radii (0.7 μm for carbon$_{Xe}$ A and 7 μm for carbon$_{Xe}$ B) as well as the accessible pores. Heating temperature for preparation affects the surface area of the resultant hard carbon. Preparation at 1273 K maintains the large surface area in carbon$_{rp}$ A (Table 2) as well as carbon$_{Xe}$ A, although the surface area is somewhat decreased by heating. It was found that heating above 1273 K did not affect the particle size and shapes as described below. Therefore, the large surface area in carbon$_{Xe}$ (and carbon$_{rp}$) A suggests the existence of the pores accessible from outer surfaces. However, preparation at 1473 K drastically decreases the surface area, implying the collapse of the pores and/or the closing of the paths into the inner space of the pores. On the other hand, the surface area in carbon sample B depends on the temperature and atmosphere of preparation (Tables 1 and 2). Xenon atmosphere leads to the drastic increase in the surface area of the hard carbon prepared at 1273 K, suggesting the formation of pores accessible from the outer surfaces. However, preparation at 1473 K decreases the surface area to 1 m^2 g^{-1}. This remarkable decrease in the surface area implies the collapse of the pores themselves or the entrance of the pores. Thus, it was found that pre-heated carbon B is carbonized effectively while maintaining the pore structure under xenon atmosphere. The ionization energy of xenon is similar to O_2, which might be the cause of higher surface area of the carbon$_{Xe}$ B sample heated at 1273 K.

Nitrogen gas adsorption–desorption isotherms of carbon$_{Xe}$ A heated at 1273 and 1473 K are presented respectively in

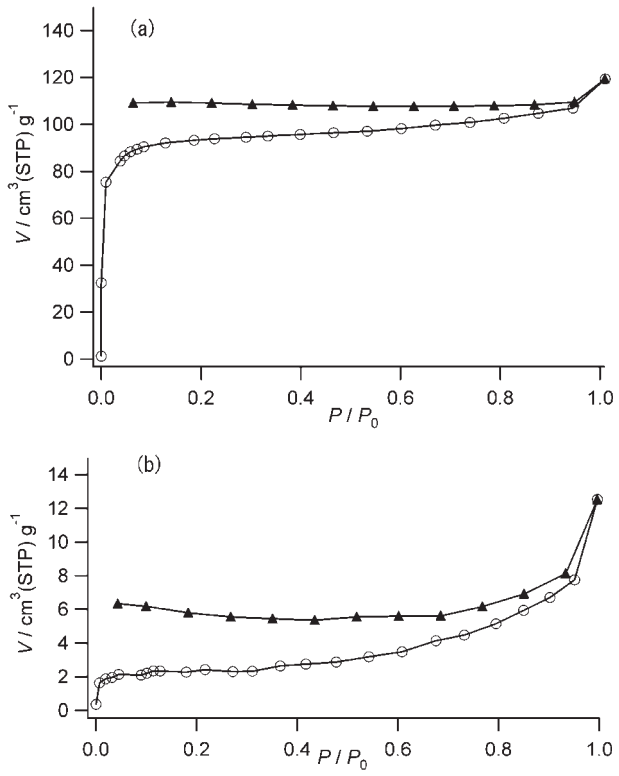

Figure 1. Adsorption (open circles) and desorption (closed triangles) isotherms of nitrogen gas on $carbon_{Xe}$ A produced by heating at 1273 (a) and 1473 K (b). Although equilibrium was not completely established for each point of isotherms because of long (over a few days or a week) adsorption or desorption time, each point was determined at the time that the adsorption or desorption reached the equilibrium in appearance.

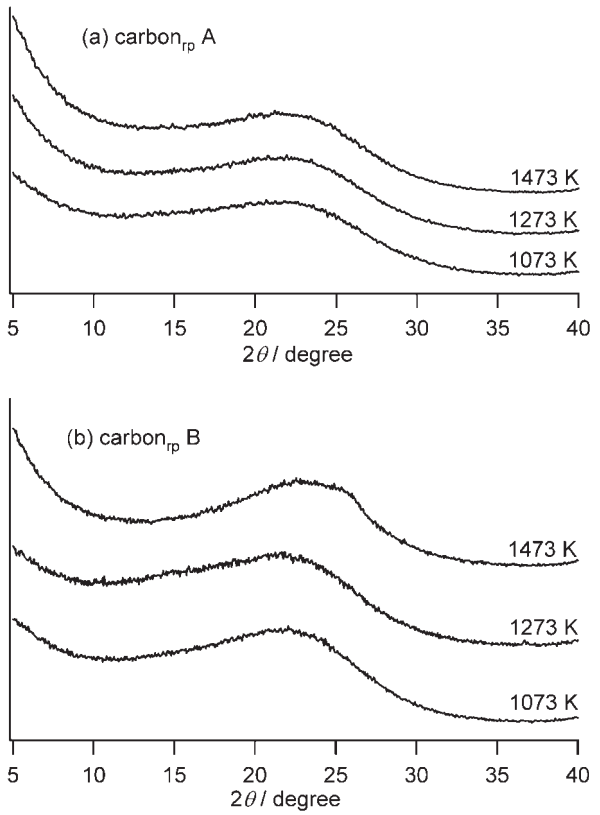

Figure 2. Powder XRD patterns of $carbon_{rp}$ A (a) and $carbon_{rp}$ B (b) produced by heating to 1073, 1273, and 1473 K.

Figures 1a and 1b. The sample heated at 1273 K showed the type I isotherm of BDDT (Brunauer, Deming, Deming, and Teller) classification, which is observed at microporous structure. Both isotherms showed marked disagreement between adsorption and desorption (hysteresis loop), and the volume of the desorption curve in Figure 1b increased with desorption under relative pressure at 0.5. The hysteresis and the increase resulted from insufficient equilibrium times (=a few minutes) for each point; consequently, they are not fundamentally associated with pore structure, for example, mesoporous structure. Furthermore, the isotherms of $carbon_{Xe}$ B prepared at 1473 K were not measurable because of small surface areas. $Carbon_{Xe}$ B prepared at 1273 K has relatively high surface area, but we could not also obtain the valuable isotherms because of the extremely long equilibrium times. The long equilibrium times (more than a few days) suggest the difficulty of N_2 diffusion between pores.

The average pore width as inferred from Horvath–Kawazoe (HK) analysis of nitrogen gas (adsorption) isotherms was estimated to be 0.97 nm for $carbon_{Xe}$ A (Figure 1a). This value is adequate or might be somewhat larger than the actual distribution of pore width because of the following two reasons; i) nitrogen gas isotherms can be used to analyze pores with diameter over 0.4 nm. In our results, contribution of such small pores has not been taken into account. The pores smaller than 0.4 nm have to be measured by other methods such as helium or high-pressure CO_2 adsorption.[51,52] ii) Insufficient equilibrium time will lead to underestimation of the adsorption of nitrogen, especially in the smaller pores, because smaller pores need longer adsorption time than larger pores generally. Therefore, the pore width estimated in our study is mainly due to the contribution of the open pores easily accessible from the outer surface.

Thus, according to the results of BET surface area and N_2 adsorption isotherms, we can conclude that the smaller surface area of $carbon_{Xe}$ B could be increased by carbonization in xenon gas. The increase in the surface area of $carbon_{Xe}$ B would be caused by formation of pore structure. In addition, most of the entrances in both $carbon_{Xe}$ A and B closed at temperatures higher than 1273 K.

XRD and Elemental Analysis. The XRD patterns for $carbon_{rp}$ samples heated at reduced pressure (ca. 0.1 Pa) are presented in Figure 2. All samples showed the characteristic patterns of hard carbon, i.e., a broad reflection around $2\theta = 23°$ which is assignable to the (002) reflection originating from a few layers of graphene sheets.[53] The d_{002} distances and the crystallite size factors (L_C) calculated from the reflection using Scherrer formula[54] are presented in Table 3. Although the surface area decreased at 1473 K, the patterns were almost identical, which suggests that the framework structure is almost unchanged, even when heated at 1473 K: only the open pores turned into closed pores. $Carbon_{Xe}$ samples heated in Xe gas showed similar diffraction patterns (not shown), which means

Table 3. The Interlayer Distances (d_{002}) and the Crystallite Size Factors (L_{C002}) Calculated from XRD(002) Reflection Using Scherrer Formula[54] (Coefficient $K = 0.9$)

Sample	Heating temperature/K	d_{002}/nm	L_{C002}/nm
$Carbon_{rp}$ A	1073	0.379	0.71
	1273	0.396	0.69
	1473	0.397	0.76
$Carbon_{rp}$ B	1073	0.401	0.70
	1273	0.403	0.67
	1473	0.377	0.83

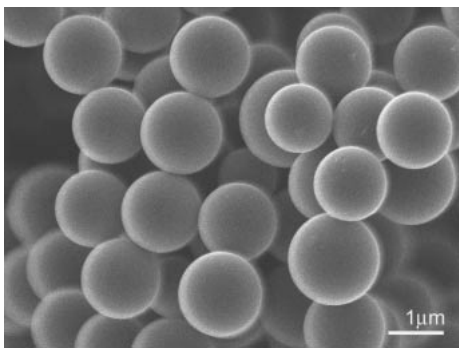

Figure 3. FE-SEM image of $carbon_{Xe}$ A produced by heating at 1073 K.

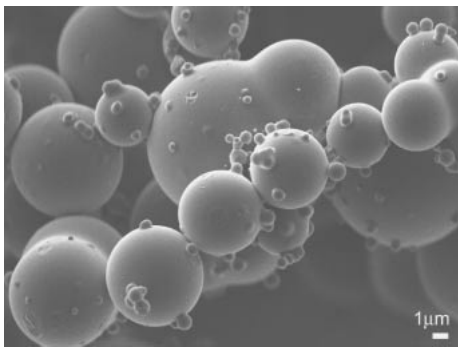

Figure 4. FE-SEM image of $carbon_{Xe}$ B produced by heating at 1073 K.

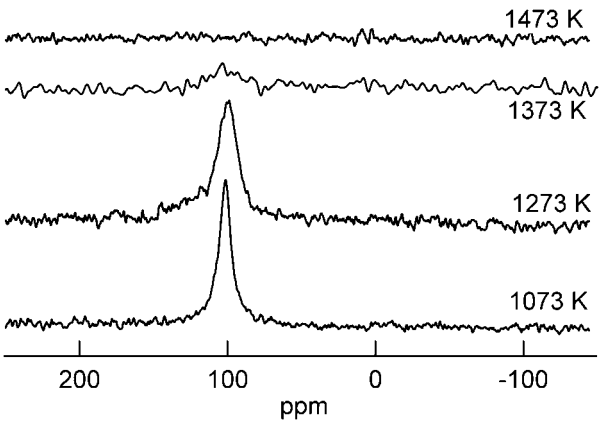

Figure 5. The ^{129}Xe NMR spectra of $carbon_{Xe}$ A produced by heating at 1073, 1273, 1373, and 1473 K in 0.1 MPa Xe atmosphere.

that the importance of the Xe atmosphere for growing the framework of carbon is negligibly small. The asymmetric (002) peak on $carbon_{rp}$ B, especially in the sample heated at 1473 K, is explainable by the distribution of particle sizes of carbon shown in SEM images (at following section). The refection of irradiated X-rays was probably disturbed by the rough surface by large particles.

The composition estimated by elemental analysis of each sample heated over 873 K was constant as $C_{1.00}O_{0.07–0.13}H_{0.12–0.32}N_{0.002–0.004}$. These results also show that the carbonization of precursor resins had been completed at 873 K.

SEM Observation. The SEM images of $carbon_{Xe}$ A and B heated at 1073 K are portrayed, respectively, in Figures 3 and 4. $Carbon_{Xe}$ A consisted of fairly homogeneous spheres whose particles were about 1.5 μm diameter. On the other hand, the sizes of spheres in $carbon_{Xe}$ B had a distribution between 1 and 15 μm and some spheres are aggregated. The sizes and shapes of carbon particles in both samples showed no remarkable changes by SEM after pre-heat treatment at 873 K.

The almost constant sizes of samples after heating to 873–1473 K support that the changes in the surface area by heat-treatment come from the changes in the pore structure of the carbon. It can be attributed to the decrease of accessible inner micropores in carbon particles by adsorbate (nitrogen or xenon gas), which is in turn caused by the isolation of pores as a result of the growing hard carbon structure.

NMR at Atmospheric Pressure. Figure 5 shows ^{129}Xe NMR spectra of $carbon_{Xe}$ A prepared under xenon atmosphere (0.1 MPa) at the following temperatures: 1073, 1273, 1373, and 1473 K. All spectra were obtained from only 1000–2000 scans. A sharp peak was observed at 101 ppm in the spectrum of a sample prepared at 1073 K, indicating the existence of the pore structure accessible by xenon atoms.[46] In this case, there are two possibilities for the origin of this resonance line; a peak resulting from the chemical exchange between the adsorbed and free xenon atoms, and a peak mainly caused by xenon in the pores without effect of free xenon gas. In the former case, it is expected that the peak position and the line width depend on the population of free xenon gas as well as the adsorbed xenon atoms.[20] In contrast to this, the resonance line depends mainly on the pore structure, i.e., pore shape, size (diameter of cylinder or width of slit), and pore volume.

The observed spectrum was affected by the heating temperature for preparation. The remarkable line broadening and the decrease in the signal intensity was found in samples prepared at higher temperature (1273 and 1373 K), and the NMR signal then disappeared in a sample prepared at 1473 K. This trend is consistent with the result of the BET surface area (the drastic decrease in the BET surface area of $carbon_{Xe}$ A prepared at 1473 K). That is, the decrease in the intensity of the ^{129}Xe NMR signal suggests the collapse of the pore structure in $carbon_{Xe}$ A prepared at 1473 K. Furthermore, the peak position was not affected by the preparation temperature between 1073 and 1373 K. These results strongly suggest that the observed resonance line is mainly caused by xenon atoms adsorbed in the pores, but not by chemical exchange between free xenon gas and the adsorbed xenon atoms. This picture is also supported by the very long time necessary to reach adsorption–desorption equilibrium in the N_2 adsorption isotherms.

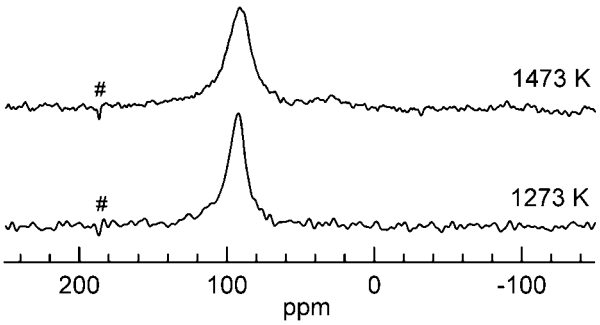

Figure 6. The ^{129}Xe NMR spectra of annealed carbon$_{Xe}$ A that was prepared by exposing carbon$_{Xe}$ A to 0.1 MPa Xe gas at 773 K for 24 h, after evacuating at 773 K for 24 h. Marks of (#) are the offset frequency of the rf pulse.

Actually, we have measured ^{129}Xe NMR spectra of carbon$_{xe}$ A and B, which were heated in Xe gas but then evacuated and sealed under helium atmosphere. The spectra showed little evidence of adsorbed xenon. Therefore, the origin of NMR signals of Figure 5 should be attributed to xenon adsorbed at "accessible" pores in carbon even if the diffusion to adsorption sites from the outer surface is very slow. In samples heated at lower temperature (under 1273 K), some pores were open pores, in other words, the pore shapes were slit (or cylinder) like. Several parts of the slit (or cylinder) like pores became narrow or collapsed under high temperature heat treatment. As a result, closed pores increase.

Figure 6 shows the ^{129}Xe NMR spectra of carbon$_{Xe}$ A after annealing (evacuation at 773 K for 1 day–exposure to 0.1 MPa Xe gas at 773 K for 1 day). A peak was visible at 92 ppm in annealed carbon$_{Xe}$ prepared at 1273 K. The line width was similar to that before annealing. Remarkably, a resonance peak was observed in annealed carbon$_{Xe}$ prepared at 1473 K. In fact, we previously reported[13] that sufficient evacuation and annealing in Xe atmosphere makes it possible to introduce xenon gas into the isolated pores existing near the surface of hard carbon particles. Appearance of the intense signal in the sample prepared at 1473 K also suggests that the pore structure existed even in the annealed carbon$_{Xe}$ A prepared at 1473 K. The annealing effectively cleaves the paths to the pores from the outer surfaces and the exposure to Xe gas at high temperature leads to the effective penetration of xenon atom into the inner space because of the large kinetic energy of xenon. Furthermore, the annealing gave rise to higher field shift from 101 to 92 ppm in both samples. The surface and/or pore structures may be a little modified by the annealing. Generally, the chemical shift reflects the xenon–wall as well as xenon–xenon interactions (vide infra). It is known that the former contribution is related to the pore size (in the case of the present samples, that is pore width). Under the same pressure condition, the comparison of the chemical shift value will give an index of the relative order of the pore size as a first approximation. Then, if the pore structure would change, the average pore size felt by xenon would be a little larger than that in the sample before annealing.

Figure 7 shows the ^{129}Xe NMR spectra in carbon$_{Xe}$ B samples prepared at 1073, 1273, 1373, and 1473 K. These were also obtained from only 1000–2000 scans. An intense

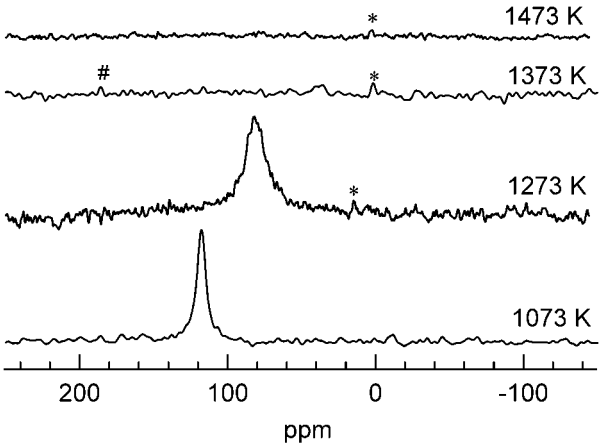

Figure 7. The ^{129}Xe NMR spectra of carbon$_{Xe}$ B heated at 1073, 1273, 1373, and 1473 K in 0.1 MPa Xe atmosphere. Marks of (#) and (*) respectively denote the offset frequency of the rf pulse and the signal of xenon gas. The signal of gas at 1273 K is not at zero ppm because of exchange interaction between xenon in gas and is adsorbed onto the sample surface.

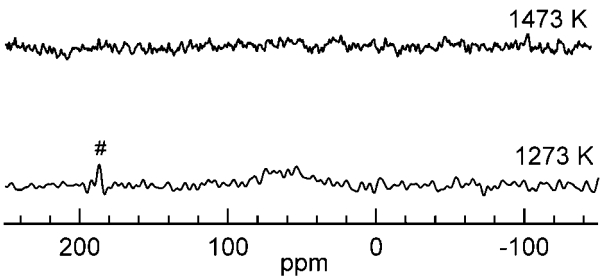

Figure 8. The ^{129}Xe NMR spectra of the carbon$_{rp}$ B heated at 1273 and 1473 K. These signals are weaker than those shown in Figure 7.

and sharp peak was observed at 118 ppm in carbon$_{Xe}$ B prepared at 1073 K, clearly indicating the pore structure of the sample. In carbon$_{Xe}$ B prepared at 1273 K, this peak shifted up-field to 82 ppm and the signal-to-noise ratio was reduced. These changes mean the increase in average pore size and decrease in pore volume, respectively. Furthermore, the NMR signal was not detected in samples prepared above 1373 K, implying the collapse of the pore structure or enclosure of the pores in these samples. In the case of carbon$_{rp}$ B prepared at 1273 K under reduced pressure ($\approx$0.1 Pa), a broad and weak signal was observed around 60 ppm. This peak was not detected in the sample prepared at 1473 K, as shown in Figure 8. The relation between the heating temperature and the ^{129}Xe NMR signal intensity is also consistent with the BET surface area in the carbon$_{Xe}$ B and the carbon$_{rp}$ B as listed in Tables 1 and 2.

Thus, it was found that the intensity of the ^{129}Xe NMR resonance line is related to the BET surface area. Since the ^{129}Xe NMR detects xenon atoms adsorbed and/or confined into the pores accessible from the outer surfaces in the carbon samples A and B, the intensity of the ^{129}Xe NMR signal gives the volume of accessible pores. This aspect also suggests that the volume of the pores accessible from the outer surface

causes the increase in the BET surface area in Tables 1 and 2. Furthermore, we found that the heating of precursors in Xe gas strengthened the NMR signal dramatically. Probably, the carbon structure grows with xenon atoms in the pores near the surface through heat treatment. The intercalated xenon diffused and made the passage to the outer surface, although the framework structures of the carbon were almost identical: XRD patterns and shapes of particles observed by FE-SEM did not change with atmospheric conditions during heating such as reduced pressure or Xe gas.

Comparison with a Hard Carbon Made from Another Precursor. The ^{129}Xe NMR chemical shift value (δ) for xenon gas adsorbed in porous materials can be expressed as[15]

$$\delta = \delta_0 + \delta_S + \delta_{Xe\text{–}Xe} \cdot \rho_{Xe} (+\delta_{SAS} + \delta_E + \delta_M) \quad (1)$$

where δ_0 is the reference (xenon gas at zero density). In addition, δ_S arises from collisions between xenon and channel surfaces, $\delta_{Xe\text{–}Xe} \cdot \rho_{Xe}$ arises from Xe–Xe collisions and is expected to be linear with Xe density under low-loading conditions.[21,46,50] Therefore the shift value at zero density is related to the pore size through the Xe–wall interaction term (δ_S). The other terms, the effect of strong adsorption sites (δ_{SAS}) at a very low level of xenon loading and the influences of electric fields (δ_E) and paramagnetic species (δ_M) are usually negligible. Actually, the ESR spectra of the present carbon samples did not display any spin signal. In eq 1, δ_S (the term of xenon–wall interaction) increases with narrowing slit-pore width, because the narrower pore width causes greater xenon–wall interaction. Therefore, the estimation of δ_S values is more effective for detailed discussion of pore width, despite a recent report by Fraissard et al.[50] which raised a query about the precise correspondence of δ_S value to the pore size for carbon materials. The δ_S values can be determined by estimating the other terms, especially $\delta_{Xe\text{–}Xe} \cdot \rho_{Xe}$ by pressure dependence measurement of NMR shift of some reported models, for example Ueda et al.[46] applying Cheung's model.[55] Although we had first attempted to estimate the δ_S values of our present samples directly through extrapolation of the pressure dependence of NMR shift, the experiment was prevented by extremely long adsorption time for each pressure. At the first approximation, the shift value at 0.1 MPa in carbon$_{Xe}$ A prepared at 1073 K leads to the rough estimation of pore size to be ca. 1 nm by comparing the reported data of similar carbon materials,[46] which seems to be in agreement with the result of nitrogen gas isotherm. However, these analyses will be less reliable for estimation of the absolute pore size. Only the relative comparison of pore sizes by NMR shift at atmospheric pressure for hard carbon samples having similar surface and component is reliable.

The ^{129}Xe NMR spectrum of samples prepared at different temperatures clearly elucidates the change of the pore structure depending on the heating temperature as well as annealing. In carbon$_{Xe}$ A, preparation temperature does not affect the peak position, while annealing causes a somewhat higher field shift of resonance lines, implying the expansion of pores. In carbon$_{Xe}$ B, the preparation temperature critically affects the peak position: The heating up to 1273 K brings about a high field shift, suggesting the expansion of pores. On the other hand, heating above 1273 K in both of carbon$_{Xe}$ A and B shows a remarkable depression of the ^{129}Xe NMR signal. On carbonization, the framework of the resin becomes amorphous consisting of graphene layers and many pores, and the resultant porous amorphous structure relaxes to hard carbon. Present study reveals that heating up to 1273 K effectively maintains the paths from the outer surface, which are accessible to xenon.

Furthermore, the pore structure of the hard carbon depends on the precursor. We have described the pressure dependence of Xe NMR for pitch-based hard carbon in a previous report:[13] Without annealing, more than 30000 scans were needed to obtain a xenon signal at micropores, even at a xenon pressure of 4.0 MPa, although the signal was not detected at all at 0.1 MPa. Annealing under Xe gas enabled detection of a stronger signal, but required more than 20000 scans. On the other hand, the present carbon made from phenolic resin B under Xe atmosphere, which has similar particle sizes to pitch-based carbon ($\approx$9 μm),[3] gives an intense signal after a few thousand scans. The resonance peak visible at 82–118 ppm in carbon$_{Xe}$ B also suggests larger pores than that in annealed pitch-based carbon, in which resonance lines appear at 128 and 29 ppm. It implies that the diffusion of xenon between neighboring pores in pitch-based carbon is more difficult than in the present carbon B because of smaller pore size and/or narrow passage between pores. Consequently, inner-pore adsorption of xenon by pitch-based carbon decreased. This aspect, which was not detectable by other methods, e.g., XRD, results in more difficult osmosis of xenon atom in pitch-based carbon.

Not only the difference between the precursors like phenolic resins and petroleum pitch, but also the difference in polymer structure of phenolic resin is expected to engender various microporous structures. We briefly reported a study using ^{129}Xe NMR for hard carbon made from another phenolic resin.[56] The carbon heated at 1473 K had smaller pores (145 ppm in the Xe NMR spectrum) than the present samples; moreover, a stoppage between pores did not occur under 1500 K because clear signals were observable up to 1473 K. The difference of the precursor composition imparts various microporous structures on hard carbon.

After all, hard carbon samples heat-treated at 1073–1473 K showed ^{129}Xe NMR signals of xenon in the pores, while the hard carbon prepared at 1273–1673 K could include lithium clusters. It is concluded that ^{129}Xe NMR examined the same pores as the space where lithium clusters are formed. In other words, our result showed that xenon can only pass through open pores composed of slit (or cylinder) like structure which is the site of forming lithium clusters, and cannot intercalate into completely isolated pores which can be observed by X-ray small-angle scattering. The small difference of heat-treatment temperature range is due to the sizes or stability of xenon and lithium atoms in carbon. Although more detailed experiments might be necessary for discovering the precise relationship between pore size forming lithium clusters and Xe NMR shift value of amorphous carbon, the transition of porous structure in a hard carbon samples by heating can be inferred from ^{129}Xe NMR analyses and production of carbon samples in a xenon atmosphere.

Conclusion

The ^{129}Xe NMR method enabled observation of xenon atoms adsorbed in pores of hard carbon samples in an equilibrium state. Consequently, the pore structures were analyzed more stably than by nitrogen adsorption–desorption isotherm measurements. Although the structures of hard carbon samples observed by XRD and FE-SEM were almost identical, the carbon made from resin A has more entrances to the inner micropore than the carbon from resin B. But the considerable entrances of both samples close at temperatures greater than 1273 K, as suggested by the surface area and ^{129}Xe NMR signal intensities. Xe NMR shifts demonstrated that the average pore size of carbon$_{Xe}$ A did not change but the size of carbon$_{Xe}$ B became larger in the heat-treated temperature range of 1073–1473 K, which is the range that lithium-clusters are observed when the carbon used as an anode of lithium ion batteries. The pore size of every hard carbon sample which we have measured from the NMR shift was obviously smaller than the pore size of 2–5 nm, which is the value for general hard carbon estimated from small-angle X-ray scattering data.

We are grateful to Mr. Niro Shiomi (Air Water Inc.) for providing phenolic resin samples and some valuable discussions related to samples. The authors thank Dr. Yoshimi Sueishi (Okayama University) for help with measuring ESR spectra. This research was partially supported by the Ministry of Education, Culture, Sports, Science and Technology Grant-in-Aid for Young Scientists (B), No. 20750166, 2008–2009. The authors also acknowledge a grant from the Foundation for Promotion of Material Science and Technology of Japan.

References

1 J. R. Dahn, A. K. Sleigh, H. Shi, B. M. Way, W. J. Weydanz, J. N. Reimers, Q. Zhong, U. von Sacken, in *Lithium Batteries: New Materials, Development and Perspectives (Industrial Chemistry Library Vol. 5)*, ed. by G. Pistoia, Elsevier, Amsterdam, **1994**, Vol. 5, pp. 1–47.

2 Y. Tanjo, T. Abe, H. Horie, T. Nakagawa, T. Miyamoto, K. Katayama, *Soc. Automot. Eng., [Spec. Publ.]SP* **1999**, *SP-1417*, 51.

3 K. Gotoh, M. Maeda, A. Nagai, A. Goto, M. Tansho, K. Hashi, T. Shimizu, H. Ishida, *J. Power Sources* **2006**, *162*, 1322.

4 E. Fitzer, W. Schaefer, S. Yamada, *Carbon* **1969**, *7*, 643.

5 T.-H. Ko, W.-S. Kuo, Y.-H. Chang, *Polym. Compos.* **2000**, *21*, 745.

6 W. S. Rothwell, *J. Appl. Phys.* **1968**, *39*, 1840.

7 K. Nishikawa, K. Fukuyama, T. Nishizawa, *Jpn. J. App. Phys.* **1998**, *37*, 6486.

8 J. Conard, P. Lauginie, *Tanso* **2000**, *191*, 62.

9 S. Gautier, F. Leroux, E. Frackowiak, A. M. Faugère, J.-N. Rouzaud, F. Béguin, *J. Phys. Chem. A* **2001**, *105*, 5794.

10 M. Letellier, F. Chevallier, C. Clinard, E. Frackowiak, J.-N. Rouzaud, F. Béguin, M. Morcrette, J.-M. Tarascon, *J. Chem. Phys.* **2003**, *118*, 6038.

11 K. Tatsumi, J. Conard, M. Nakahara, S. Menu, P. Lauginie, Y. Sawada, Z. Ogumi, *J. Power Sources* **1999**, *81–82*, 397.

12 M. Nagao, C. Pitteloud, T. Kamiyama, T. Otomo, K. Itoh, T. Fukunaga, K. Tatsumi, R. Kanno, *J. Electrochem. Soc.* **2006**, *153*, A914.

13 K. Gotoh, T. Ueda, H. Omi, T. Eguchi, M. Maeda, M. Miyahara, A. Nagai, H. Ishida, *J. Phys. Chem. Solids* **2008**, *69*, 147.

14 P. J. Barrie, J. Klinowski, *Prog. Nucl. Magn. Reson. Spectrosc.* **1992**, *24*, 91.

15 M.-A. Springuel-Huet, J.-L. Bonardet, A. Gédéon, J. Fraissard, *Magn. Reson. Chem.* **1999**, *37*, S1.

16 T. Ito, J. Fraissard, Proceedings of the 5th International Conference on Zeolites, **1980**, p. 510.

17 J. Demarquay, J. Fraissard, *Chem. Phys. Lett.* **1987**, *136*, 314.

18 J. A. Ripmeester, C. I. Ratcliffe, *J. Phys. Chem.* **1990**, *94*, 8773.

19 I. L. Moudrakovski, C. I. Ratcliffe, J. A. Ripmeester, *J. Am. Chem. Soc.* **1998**, *120*, 3123.

20 N. Kato, T. Ueda, H. Omi, K. Miyakubo, T. Eguchi, *Phys. Chem. Chem. Phys.* **2004**, *6*, 5427.

21 H. Omi, T. Ueda, N. Kato, K. Miyakubo, T. Eguchi, *Phys. Chem. Chem. Phys.* **2006**, *8*, 3857.

22 M.-A. Springuel-Huet, F. Guenneau, A. Gédéon, A. Corma, *J. Phys. Chem. C* **2007**, *111*, 5694.

23 Y. Kawata, Y. Adachi, S. Haga, J. Fukutomi, H. Imai, A. Kimura, H. Fujiwara, *Anal. Sci.* **2007**, *23*, 1397.

24 Y. Liu, W. Zhang, Z. Liu, S. Xu, Y. Wang, Z. Xie, X. Han, X. Bao, *J. Phys. Chem. C* **2008**, *112*, 15375.

25 A. Nossov, E. Haddad, F. Guenneau, A. Gédéon, *Phys. Chem. Chem. Phys.* **2003**, *5*, 4473.

26 A. Nossov, F. Guenneau, M.-A. Springuel-Huet, E. Haddad, V. Montouillout, B. Knott, F. Engelke, C. Fernandez, A. Gédéon, *Phys. Chem. Chem. Phys.* **2003**, *5*, 4479.

27 M. A. Springuel-Huet, J. Fraissard, R. Schmidt, M. Stocker, W. C. Conner, *Spec. Publ.—R. Soc. Chem.* **1997**, *213*, 452.

28 T. Koskela, J. Jokisaari, C. Satyanarayana, *Microporous Mesoporous Mater.* **2004**, *67*, 113.

29 H. Omi, B. Nagasaka, K. Miyakubo, T. Ueda, T. Eguchi, *Phys. Chem. Chem. Phys.* **2004**, *6*, 1299.

30 Y. Liu, W. Zhang, S. Xie, L. Xu, X. Han, X. Bao, *J. Phys. Chem. B* **2008**, *112*, 1226.

31 A. Gil, S. A. Korili, M. A. Vicente, *Catal. Rev.—Sci. Eng.* **2008**, *50*, 153.

32 J. A. Ripmeester, D. W. Davidson, *J. Mol. Struct.* **1981**, *75*, 67.

33 I. L. Moudrakovski, A. A. Sanchez, C. I. Ratcliffe, J. A. Ripmeester, *J. Phys. Chem. B* **2001**, *105*, 12338.

34 I. L. Moudrakovski, A. Sanchez, C. I. Ratcliffe, J. A. Ripmeester, *J. Phys. Chem. B* **2000**, *104*, 7306.

35 A. P. M. Kentgens, H. A. Van Boxtel, R. J. Verweel, W. S. Veeman, *Macromolecules* **1991**, *24*, 3712.

36 M. Tomaselli, B. H. Meier, P. Robyr, U. W. Suter, R. R. Ernst, *Chem. Phys. Lett.* **1993**, *205*, 145.

37 B. Nagasaka, T. Eguchi, H. Nakayama, N. Nakamura, Y. Ito, *Radiat. Phys. Chem.* **2000**, *58*, 581.

38 H. Ago, K. Tanaka, T. Yamabe, T. Miyoshi, K. Takegoshi, T. Terao, S. Yata, Y. Hato, S. Nagura, N. Ando, *Carbon* **1997**, *35*, 1781.

39 Y. J. Lee, K.-D. Park, S.-J. Huang, S.-B. Liu, H.-J. Lee, *J. Nanosci. Nanotechnol.* **2007**, *7*, 3932.

40 T. Suzuki, M. Miyauchi, M. Takekawa, H. Yoshimizu, Y. Tsujita, T. Kinoshita, *Macromolecules* **2001**, *34*, 3805.

41 M. S. Syamala, R. J. Cross, M. Saunders, *J. Am. Chem. Soc.* **2002**, *124*, 6216.

42 M. Frunzi, R. J. Cross, M. Saunders, *J. Am. Chem. Soc.*

2007, *129*, 13343.
43 J. M. Kneller, R. J. Soto, S. E. Surber, J. F. Colomer, A. Fonseca, J. B. Nagy, G. Van Tendeloo, T. Pietraß, *J. Am. Chem. Soc.* **2000**, *122*, 10591.
44 K. V. Romanenko, A. Fonseca, S. Dumonteil, J. B. Nagy, J.-B. d'Espinose de Lacaillerie, O. B. Lapina, J. Fraissard, *Solid State Nucl. Magn. Reson.* **2005**, *28*, 135.
45 K. V. Romanenko, P. A. Simonov, O. G. Abrosimov, O. B. Lapina, A. Fonseca, J. B. Nagy, J.-B. d'Espinose, J. Fraissard, *React. Kinet. Catal. Lett.* **2007**, *90*, 355.
46 T. Ueda, H. Omi, T. Yukioka, T. Eguchi, *Bull. Chem. Soc. Jpn.* **2006**, *79*, 237.
47 D. J. Suh, T. J. Park, S. K. Ihm, R. Ryoo, *J. Phys. Chem.* **1991**, *95*, 3767.
48 K. V. Romanenko, X. Py, J.-B. d'Espinose de Lacaillerie, O. B. Lapina, J. Fraissard, *J. Phys. Chem. B* **2006**, *110*, 3055.
49 K. Saito, A. Kimura, H. Fujiwara, *Magn. Reson. Imaging* **2003**, *21*, 401.
50 K. V. Romanenko, J.-B. d'Espinose de Lacaillerie, O. Lapina, J. Fraissard, *Microporous Mesoporous Mater.* **2007**, *105*, 118.
51 D. Lozano-Castelló, D. Cazorla-Amorós, A. Linares-Solano, D. F. Quinn, *J. Phys. Chem. B* **2002**, *106*, 9372.
52 D. Lozano-Castelló, D. Cazorla-Amorós, A. Linares-Solano, *Carbon* **2004**, *42*, 1233.
53 R. E. Franklin, *Proc. R. Soc. London, Ser. A* **1951**, *209*, 196.
54 A. L. Patterson, *Phys. Rev.* **1939**, *56*, 978.
55 T. T. P. Cheung, *J. Phys. Chem.* **1995**, *99*, 7089.
56 K. Gotoh, A. Nagai, in *Amorphous Materials: Research, Technology and Applications*, ed. by J. R. Telle, N. A. Pearlstine, Nova Science, New York, **2009**, in press.